Layered Microstructures based on $BaZr_{0.85}Y_{0.15}O_{3-\delta}$ by Pulsed Laser Deposition for Metal Supported Proton Ceramic Electrolyzer Cells

Elena Stefan[1*], Marit Stange[2], Christelle Denonville[2], Yngve Larring[2], Nicolas Hildenbrand[3] Truls Norby[1] and Reidar Haugsrud[1]

1 University of Oslo, Department of Chemistry, FERMiO, Gaustadalléen 21, NO-0349 Oslo, Norway

2 SINTEF, Forskningsveien 1, NO-0373 Oslo, Norway

3 Solmates BV, Drienerloolaan 5, Building 46, 7522NB, Enschede, the Netherlands

E-mail addresses: elena.stefan@smn.uio.no; marit.stange@sintef.no; Christelle.Denonville@sintef.no; Yngve.Larring@sintef.no; Nicolas.Hildenbrand@solmates.nl; truls.norby@kjemi.uio.no; reidar.haugsrud@smn.uio.no

* Corresponding author. Tel.: +47 22 85 77 59; fax +47 22 84 06 51.

Abstract

Planar metal-supported cell designs provide cost-effective scaling-up of solid oxide fuel cells and electrolyzers. Here, we report on the fabrication of a $BaZr_{0.85}Y_{0.15}O_{3-\delta}$–NiO (BZY15-NiO) composite electrode and $BaZr_{0.85}Y_{0.15}O_{3-\delta}$ (BZY15) proton conducting electrolyte films on metal and ceramic substrates using pulsed laser deposition (PLD). The results demonstrate successful sequential deposition of porous electrode and dense electrolyte structure by PLD at moderate temperatures, without the need for subsequent high temperature sintering. The decrease in roughness of the metal substrate used for deposition by spray-coating intermediary oxide layers had significant importance to the fabrication of functional layers as thin films. Crystalline porous BZY15-NiO and dense BZY15 films were sequentially deposited at high substrate temperature on metal supports (MS) with or without an electron-conducting barrier oxide layer, e.g. MS/(BZY15-Ni)/(BZY15-NiO)/BZY15 and MS/CeO_2/(BZY15-NiO)/BZY15. The different microstructures for electrode and electrolyte were achieved with deposition steps at different substrate temperatures (800, 600 °C) and a gradual decrease of the pressure of O_2 in the deposition chamber.

Keywords: pulsed laser deposition (PLD), thin films, sequential deposition, metal support, proton ceramic electrolyzer cells (PCEC).

1 Introduction

Storage of peak electricity as fuels or other valuable chemicals greatly promote utilization of renewable energy sources .[1, 2] In this context, high-temperature electrolysis offers high efficiency for hydrogen or syngas production at temperatures of around 600 °C. Lowering the operating temperatures of these devices would further increase their practicality, by enabling for example the use of less expensive materials in the cell assembly, such as steel-based interconnects and metal-supported electrodes. As reported previously, a decrease in operating temperature and additional performance enhancements can be achieved by decreasing electrolyte thickness and by employing proton conducting electrolyte materials that exhibit high proton conductivity with low activation energies for intermediate temperature range.[3–5]

$BaZr_{0.85}Y_{0.15}O_{3-\delta}$ (BZY15) has been studied extensively as electrolyte for proton ceramic fuel cells (PCFCs) and proton ceramic electrolyzer cells (PCECs). [4–15] It was found that BZY15 has relatively high bulk proton conductivity and chemical stability in steam or CO_2 containing atmospheres.[6, 7] Fabrication of metal supported proton ceramic electrolyzer cells (MS-PCEC) based on barium zirconate is challenging due to the poor sintering ability of the BZY and the limitations imposed by the metal support (low sintering temperature of the metal < ~1300 °C, sintering under reducing conditions for all functional layers). Low temperature fabrication techniques, such as pulsed laser deposition (PLD) or magnetron sputtering are alternatives to overcoming the high temperature sintering step required for the BZY15 electrolyte layer and to decrease the electrolyte thickness. Additionally, the columnar textured microstructure formed by PLD alleviates grain boundary resistance and has shown higher ionic conductivity for BZY15 processed by PLD. [12]

PLD produces films of complex oxides with the advantage of reproducing the target stoichiometry in the film. A high energy laser beam hits the target at a pre-set energy and the target material is vaporized, forming the plasma plume. Because of collisions with the gas molecules, the plasma plume is decelerated but a fraction of the particles still have enough kinetic energy to reach the substrate, which is located at a fixed distance from the target. PLD is a common technique for fabrication of micro-SOFCs and it proved to be a versatile method for material processing at lower temperatures, e.g. microstructure optimization of deposited layers as cathode or electrolyte.[12, 16–21] Micro-SOFCs have demonstrated remarkable performances at low temperatures (1 W cm^{-2} at 500 °C)[22, 23]. Integration of cell components obtained by PLD on currently available fuel cell/ electrolyzer cell platforms (anode supports, metal supports) are somewhat challenging, but successful results were reported recently on the deposition of thin electrolyte layers on porous BZY-NiO electrode supports.[17, 24–26]

This work provides insight into effects of PLD parameters, such as substrate temperature and deposition pressure, on growth of porous BZY15-NiO and dense BZY15 polycrystalline films with or without Y_2BaNiO_5 (BYN) sintering aid. The films were deposited on polycrystalline ceramic substrates such as BZY15-NiO, CeO_2 or $La_{0.5}Sr_{0.5}Ti_{0.75}Ni_{0.25}O_{3-\delta}$ (LSTN) [27] to study chemical compatibility, adherence, interfaces and crystallinity. Results were transferred towards facilitating the integration of electrode and electrolyte films on metal/ceramic substrates.

2 Experimental

The BZY15 or BZY15-BYN electrolyte films were deposited on BZY15-NiO or CeO_2 pellets, Al_2O_3 polycrystalline substrates (MTI, P > 96%), and on metallic substrates. BZY15-NiO and CeO_2 pellets were prepared by uniaxial pressing of BZY15-NiO (60 – 40 vol. %, CerPoTech) or CeO_2 (Aldrich, > 500 nm) powders, followed by sintering at 1400 °C for 6 h and at 1100 °C for 5 h, respectively. Pellets were polished with SiC paper and diamond paste down to 0.25 µm, cleaned ultrasonically in isopropanol and deionised water, and dried at 120 °C. Al_2O_3 substrates were annealed at 1300 °C for 10 h and polished and cleaned using the same procedure.

Metallic substrates (MS) (Fe/Cr 20.6% with Si < 0.08%) were obtained by aqueous tape casting as described in [28]. BZY-NiO (60 – 40 vol.%, CerPoTech), CeO_2 (Aldrich, > 500 nm) or $La_{0.5}Sr_{0.5}Ni_{0.25}Ti_{0.75}O_3$ (LSTN) synthesized by the citric acid method were mixed with organic solvents to form slurries, spray-coated (≥ 10 layers) on the sintered MS and thermally treated in reducing atmosphere (4%H_2/Ar) at temperatures of 1100 – 1300 °C for 1-2 h. For improved reproducibility of the samples, a bigger batch of LSTN was acquired from CerPoTech to be applied on the metal supports by spray coating. A detailed characterization of these samples, including electrochemical characterization, will be published elsewhere.

BZY15 ceramic targets were prepared from commercial powder (CerPoTech), or powder prepared by solid state reactive sintering (SSRS)[9–11], without and also with Y_2BaNiO_5 (BYN) as sintering aid. The target prepared with sintering aid reached 98% relative density when sintered at 1500 °C, while the target without sintering aid was sintered at 1600 °C and had relative densities of ~80% using the CerPoTech BZY15 powder. Films were prepared using a PLD workstation (SURFACE systems+technology GmbH & Co. KG, Germany, with a COMPex *Pro* 205, Coherent, KrF excimer laser, λ = 248 nm and pulse length of 25 ns). Prior to deposition, the chamber was evacuated to basis pressure (5 x 10^{-6} mbar). Samples were heated in the temperature range of 600-800 °C. The energy density was set to 1.0-1.6 J cm^{-2}, laser frequency 5-7 Hz and target-substrate distance (TSD) kept constant at 6 cm. Ramp rates and O_2 partial pressures for heating and cooling steps are listed in

Table 1 and Table 2. Deposition rates were determined after the most favourable conditions for deposition were established, such as new fill of laser gas, cleaned laser window and polished target surface. XRD patterns on BZY15 films were collected, using the grazing incidence angle method with parallel beam geometry, on a PANalytical Empyrean X-ray diffractometer (CuKα radiation) equipped with a Proportional detector Xe. The data were collected at an incidence beam angle of ω = 1°, for 2θ from 10° to 120°. Film microstructure and grain growth were analysed on a FEI Quanta 200 FEG-ESEM scanning electron microscope. Film thickness was determined using ImageJ open source image processing software.[29, 30] Evaluation of film thickness from cross-section micrographs was averaged for 8 – 12 readings.

3 Results and discussion

For a better understanding of the relation between film microstructure (dense, porous) and the deposition parameters, (e.g. the substrate temperature and ambient O_2 pressure), BZY15 and BZY15-NiO films were studied on BZY15-NiO or CeO_2 pellets at temperatures of 600 – 800 °C and different pressures (0.02 – 0.1 mbar O_2). The deposition conditions and substrates are listed in Table 1. BZY-NiO and CeO_2 were selected as substrates for compatibility and crystallinity studies, since the same oxides were applied as intermediary layers on the porous MS, as described in the Experimental part and section 3.4.

3.1 BZY15 electrolyte films deposited on BZY15-NiO substrates

XRD patterns of BZY15 and BZY15-BYN films, with thicknesses of ~2 µm, deposited at 800 °C and 0.02 mbar O_2 (Figure 1) were collected in grazing angle mode (GI-XRD) and confirmed the formation of single phase, crystalline films. Peak positions correspond to BZY15, perovskite with cubic crystal structure with a symmetry described by the space group Pm-3m (no. 221). The relative intensities of the peaks are comparable with a BZY15 powder sample, indicating that no significant crystallographic texturing is present in the films. As expected, the use of polycrystalline substrates resulted in formation of BZY15 polycrystalline films. Cell parameters were determined from Rietveld refinement, with a = 4.2076 Å for BZY15 and a = 4.2176 Å for BZY15-BYN and are in a good agreement with reported values of BZY prepared by powder processing techniques.[10, 31–33] XRD patterns were collected also for samples deposited at 600 and 450 °C (not shown) and confirmed formation of crystalline films even for deposition at as low temperature as 450 °C.

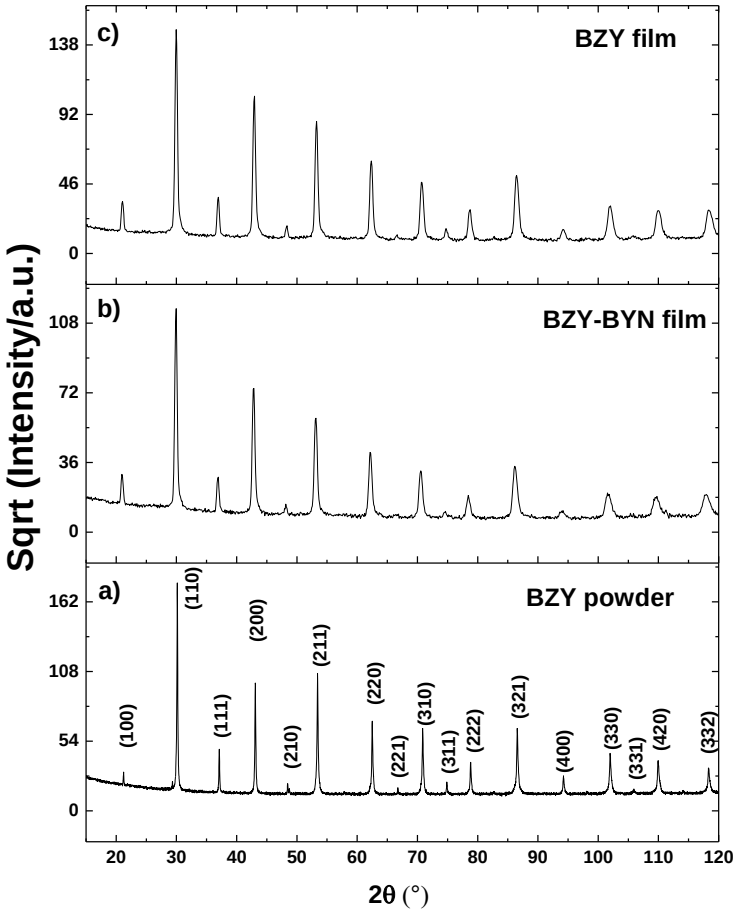

Figure 1 X-ray diffraction pattern of: a - BZY15 powder collected in reflection mode; b – BZY15-BYN film, c – BZY15 film collected in grazing angle geometry (grazing angle 1°).

The micrographs in Figure 2 display the cross-section of two BZY15 films deposited at 1.6 J cm^{-2} (Figure 2 a) and 1 J cm^{-2} (Figure 2 b), showing that dense microstructures were obtained for both films. The BZY15 film deposited at higher laser energy is ~5.4 µm thick with randomly orientated grains, while the film deposited with lower laser energy is ~2.5 µm thick and it shows smooth, columnar grains. For higher laser energy, the fractured film is rather rough indicating that the high deposition rate limited the columnar growth, leaving the grains randomly oriented. At intermediate laser energies (1.2, 1.4 J cm^{-2}) deposited films showed columnar grains, with clear grain boundaries. Chang et al. [20] and Infortuna et al. [21] described in detail the influence of deposition conditions for the microstructure and crystallinity of BZY20 and yttria stabilized zirconia (YSZ) films, respectively. The authors reported that BZY20 and YSZ dense electrolyte films were obtained when deposited under low ambient pressure and high temperatures of the substrate (above 500 – 600 °C).

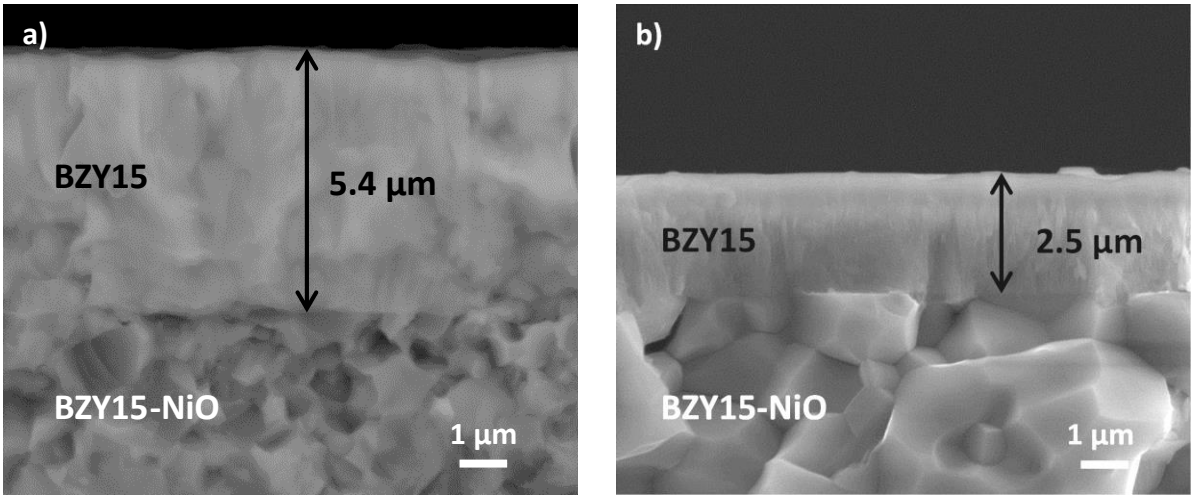

Figure 2 Cross-section micrographs of BZY15 dense films deposited at 800 °C, 0.02 mbar O_2 and laser energy: a) 1.6 J cm^{-2}; b) 1.0 J cm^{-2}. (Images collected in mix signal (SEI+ BSE electrons)).

BZY15 dense films showed good compatibility with the BZY15-NiO substrates, with no delamination or cracking. The most appropriate microstructure and crystallinity of the electrolyte films were obtained for pressures ≤ 0.02 mbar O_2 at 600 and 800 °C. Higher laser energy resulted in increased deposition rate and thicker films with randomly oriented grains. Lower energies resulted in lower deposition rates and thinner films with columnar grains, as desired for MS-PCEC electrolyte.

3.2 BZY15-NiO electrode films deposited on CeO_2 substrates

The compatibility of BZY15 electrolyte and BZY-NiO electrode films was tested also for CeO_2 pellets, for which the deposition parameters from the previous samples were used successfully. BZY-NiO electrode was deposited on a CeO_2 pellet at a substrate temperature of 800 °C in 0.1 mbar O_2. The resulting film had columnar grains (Figure 3 a, b) and a moderate porosity. When deposited at 800 °C and ambient pressure lower than 0.1 mbar O_2, the BZY-NiO film was denser than preferred for an electrode microstructure (micrograph not shown). After annealing in air at 1100 °C for 2 h, the porosity of the BZY-NiO layer became more visible, seemingly due to the crystal growth of individual phases (Figure 3 c, d). Noh et al. [24, 25] and Muecke et al. [34, 35] reported the nano-crystalline nature of the "as-deposited" NiO-YSZ and Ni/gadolinia-doped ceria (CGO) composite electrodes by PLD. They found that Ni agglomeration was suppressed for samples annealed in air at temperatures of 800 – 1000 °C, by allowing crystal growth for the two phases before reduction. Although this step would assure an appropriate electrode microstructure and address the Ni agglomeration issue,

metal supports exclude the possibility of annealing in air at high temperatures of 1000 – 1100 °C, considering the poor oxidation resistance of the FeCr steel at these temperatures. Therefore, the electrodes should be optimized by tuning the deposition conditions and crystal growth favoured by an additional annealing step.

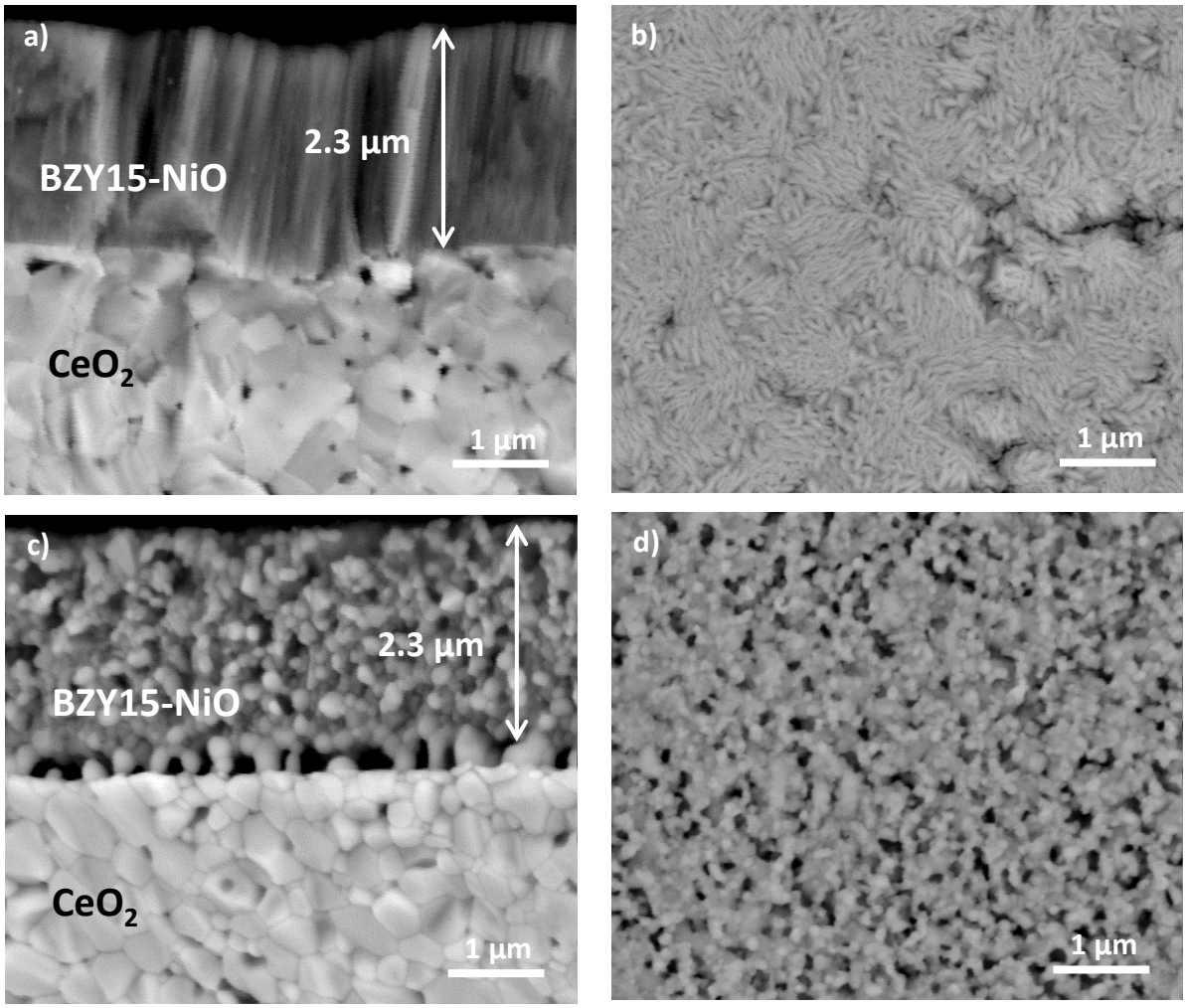

Figure 3 Cross-section and surface micrographs of BZY-NiO on CeO_2 pellets: a, b – as-deposited (800 °C, 0.1 mbar O_2), cross-section and surface; c, d –cross-section and surface after annealing in air at 1100 °C for 2 h. (Images collected in backscattering mode.)

For the BZY-NiO electrode and BZY15-BYN electrolyte layers sequentially deposited on CeO_2 pellets, the BZY-NiO film was denser than when deposited as a single layer, due to the prolonged exposure at 800 °C. BZY-NiO was deposited as described above (substrate temperature 800 °C, 0.1 mbar O_2, Table 1), while the BZY15-BYN film was deposited at lower ambient pressure, 0.02 mbar

O_2, to improve densification. Substrate temperature, target-substrate distance, frequency and laser energy were kept constant. Columnar growth was observed for the electrode layer, while the grains in the electrolyte film showed a transition from columnar to random orientation (Figure 4 a), possibly related to an orientation change, dependent on film thickness. Such an effect was observed and studied in detail for $La_{1.875}Sr_{0.125}NiO_4$ thin films (25 – 150 nm) deposited on $SrTiO_3$ single crystals [36] and for Ni thin films (13 – 360 nm) deposited on YSZ single crystals [37]. Upon reduction, at 700 °C / 5 h in $5H_2$/Ar, NiO formed metallic Ni particles and nano-porosity. The thickness of the two layers decreased and a clear interface between the cathode and electrolyte was formed after reduction (Figure 4 b, c). Longer exposure at high temperature (700 °C) improved the crystal growth in the electrolyte, leading to formation of smooth columnar grains. However, some areas of the cross-section showed porosity in the electrolyte layer after reduction and surface micrographs confirmed formation of cracks, induced by Ni formation and agglomeration in the electrode layer. Reduction of the cathode film after deposition, without annealing in air, led to Ni agglomeration and insufficient porosity. The stability of BZY-BYN electrolyte upon reduction was further investigated for BZY-BYN deposited as individual layers on commercial Al_2O_3 polycrystalline substrate and reduced at 650 °C for 18 h, in $5H_2$/Ar. On Al_2O_3 substrate, the electrolyte layer remained integer, without cracks or porosity, and only few Ni particles were observed on the surface and in cross-section (Figure 5). Such small amount of Ni present in the BYN sintering aid may be accommodated without causing cracks in the electrolyte membrane, since only one side of the electrolyte is exposed to reducing conditions, while the other side is exposed to air during tests under realistic operating conditions.

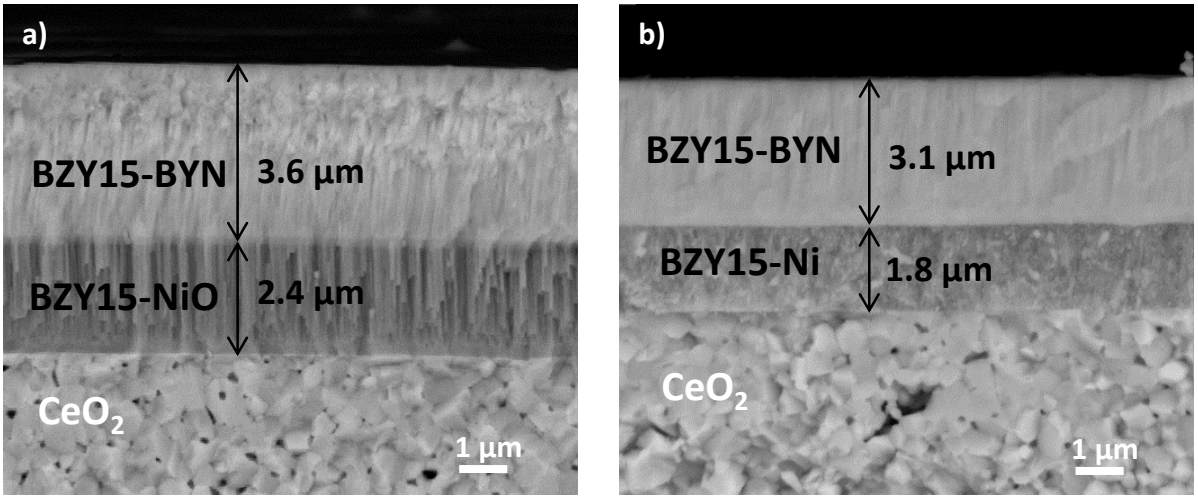

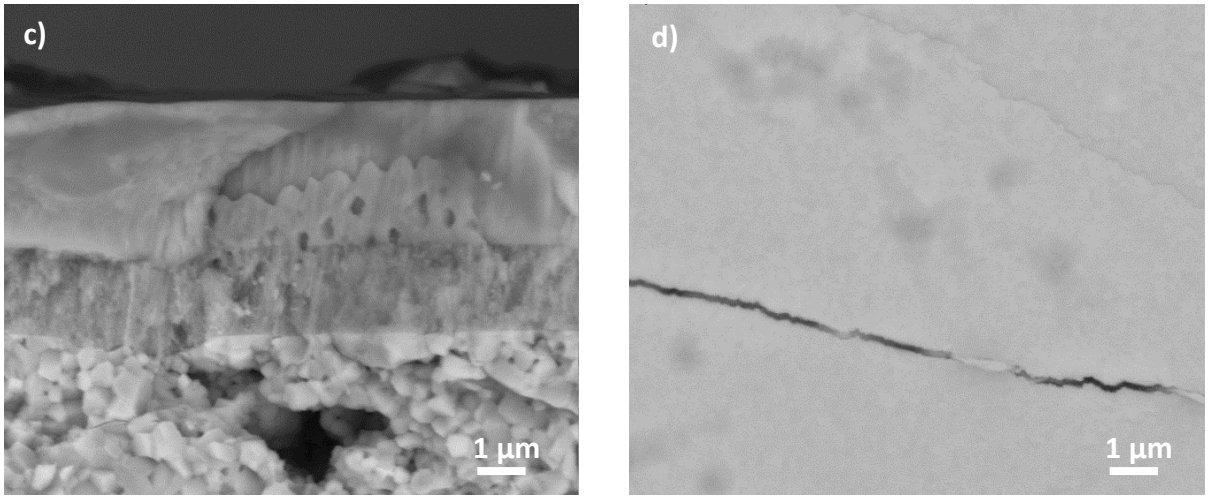

Figure 4 Cross-section and surface micrographs of: a – electrode (BZY-NiO, 60-40 vol %) and electrolyte (BZY-BYN) layer deposited on CeO_2 substrate; b, c – electrode and electrolyte layer after reduction at 700 °C / 5 h, with detail; (Images collected in backscattering mode.)

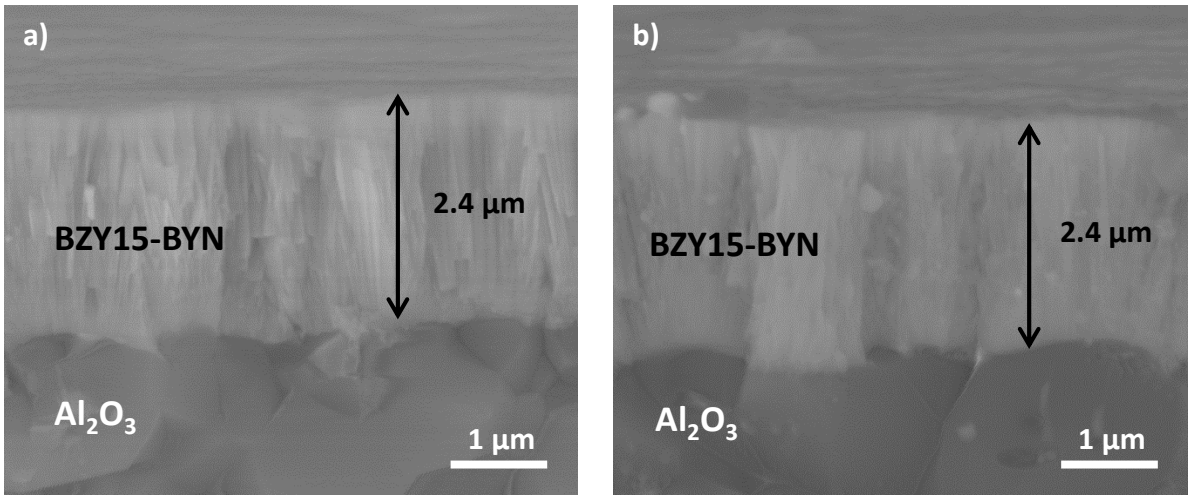

Figure 5 Cross-section and surface micrographs of: a – BZY-BYN electrolyte deposited on Al_2O_3 at 800 °C and b – BZY-BYN electrolyte after reduction in 5%H_2/Ar at 650 °C for 18 h. Images collected in mixed signal (SEI+ BSE electrons).

3.3 Influence of deposition parameters and substrate on film morphologies

The influences of pressure and temperature on the microstructure have been studied by Thornton [38] for metallic coatings deposited by sputtering. It was found that lower ambient

pressure and increased temperature yielded densification of the deposited material with columnar grains. Lower temperatures and higher ambient pressure resulted in porous layers of columnar grains, where the individual grains had near bulk density. These observations were confirmed also for ceramic layers deposited by PLD, such as BZY films [20], YSZ [21], BZY-NiO films [24–26] and even for $La_{0.58}Sr_{0.4}Co_{0.2}Fe_{0.8}O_{3-\delta}$ (LSCF) [39]. As reported in these studies, a feasible method for obtaining porous films, in our case BZY-NiO electrode, is to initiate columnar grains by deposition at intermediate to high ambient pressures (~0.1 – 0.25 mbar) and relatively low temperatures (below 400 °C). A post-annealing step at higher temperatures was found to increase film crystallinity, without significant densification of the film. A second option for deposition of porous electrode films, as applied in the present study, is the deposition at high ambient pressure directly at higher substrate temperatures of 600 – 800 °C. Noh et al. [24] found that BZY-NiO electrode films deposited at low temperature and annealed at 700 °C had poor crystallinity that resulted in low conductivity, while the films deposited on substrate at 700 °C had good crystallinity and good electrical conductivity. These findings support the deposition of BZY15-NiO at increased substrate temperature as an appropriate method for obtaining electrode films with improved performance.

Table 1 Deposition conditions for BZY15 and BZY-NiO films on ceramic substrates

E (J/cm^2)	F (Hz)	P (mbar)	T (°C)	TSD (cm)	Substrate
1.6	5	0.02	800	6	BZY-NiO
1.0	5	0.02	800	6	BZY-NiO
1.2	5	0.02	800	6	Al_2O_3
1.2	5	0.10	800	6	CeO_2
1.2	5	0.10	800	6	CeO_2
	5	0.02	800	6	

In summary, BZY15-NiO and BZY15-BYN films showed good adherence to the CeO_2 dense pellets, during deposition and reduction steps. The presence of a small amount of Ni led to formation of cracks in the electrolyte layer during reduction. When annealed in air at 1100 °C, the BZY15-NiO electrode showed dewetting and loss of adherence from the CeO_2 substrate. Both annealing in air of BZY15-NiO and the use of BZY15-BYN electrolyte layer are found to be unfeasible options for further processing of MS-PCECs. However, post-deposition annealing at 700 °C resulted in an improved microstructure of the electrolyte film, with formation of columnar grains.

3.4 Integration of oxide thin films on metallic substrates

Metal supports (MS) used for deposition by PLD of cathode and electrolyte type layers were coated for improving oxidation resistance, as described in ref [28]. Oxide spray-coated layers e.g. BZY-NiO, CeO_2 or LSTN were added to decrease the surface roughness of the MS and to facilitate formation of continuous films by PLD. The metal/ceramic substrates MS/(BZY-Ni), MS/CeO_2 and MS/LSTN were sintered under reducing conditions. The BZY-Ni layer sintered in reducing atmosphere resulted in a highly porous microstructure and poorly sintered ceramic layer, while MS/CeO_2 and MS/LSTN formed uniform, nano-porous layers, with grain size < 500 nm.

Lanthanum strontium titanates with exsolved Ni particles or infiltrated with Ni- gadolinia doped ceria (CGO) have been studied as alternative materials to YSZ-Ni hydrogen electrodes for solid oxide cells (SOFCs, SOECs) and shown to be efficient electrode materials with reasonable catalytic activity.[27, 40, 41] Reported results on $La_{0.5}Sr_{0.5}Ni_{0.25}Ti_{0.75}O_{3-\delta}$, (LSTN)[27] indicate this material as a good candidate for intermediary or electrode layer between the metal substrate and other thin film cell components implemented by PLD. Arrivé et al. [27] reported LSTN as an orthorhombic perovskite with space group Imma and cell parameters a = 5.5285 Å b = 5.5583 Å and c = 7.81113 Å. In the present study, XRD analysis of the as-prepared sample confirmed the formation of single phase perovskite while the XRD of the reduced material (bottledry 4% H_2/Ar at 1225 °C for 2 h), showed segregation of secondary phases La_2TiO_5, La_2O_3 and Ni.[27]. Reduced MS/LSTN had porosity and particle agglomerates in the micron range, but still appropriate microstructure for BZY15 electrolyte deposition by PLD.

Densification of BZY15 film was achieved when lower ambient pressure was used for deposition on MS/(BZY-Ni) substrates. Initially, BZY-NiO was deposited on top of the spray coated BZY-Ni at 800 °C in O_2, 0.25 and 0.15 mbar. Electrolyte densification was achieved by gradually decreasing the ambient pressure, while the substrate temperature was also decreased to 600 °C (Figure 6). Even though a densified BZY15 layer was obtained on MS/(BZY-Ni), it was not continuous as a result of the relatively high roughness and porosity of the spray coated layer.

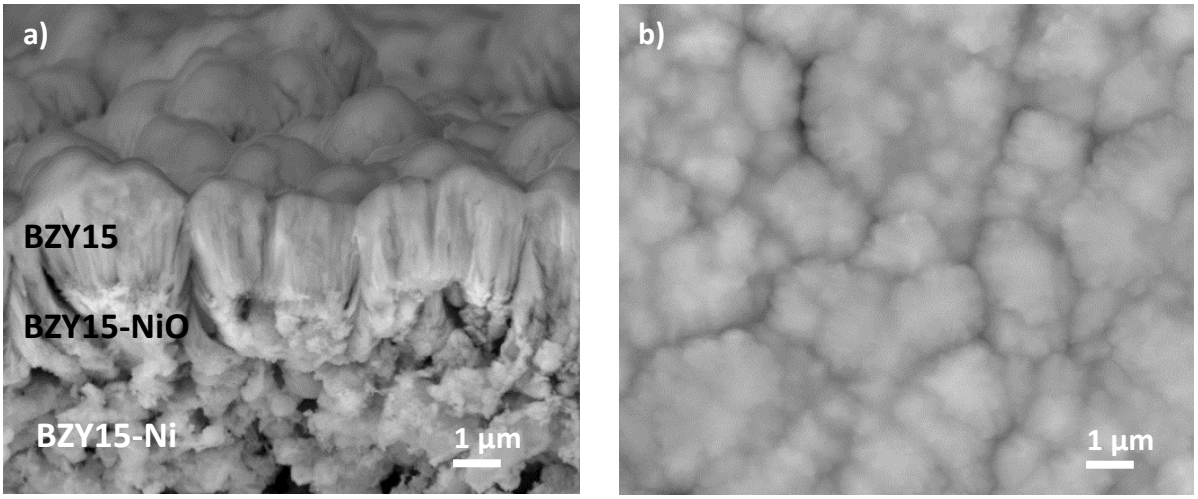

Figure 6 Cathode and electrolyte deposited on MS/(BZY-Ni) substrate deposited at different temperatures (800, 600 °C) and gradual decrease of the ambient pressures from 0.25, 0.15, 0.1, 0.02 and 0.002 mbar O_2.

Cathode and electrolyte deposited on MS/CeO_2 substrates were obtained as separate films, with different microstructure, when deposited under different conditions: temperatures (800 °C for cathode and 600 °C for electrolyte deposition) and different pressures. When deposited at the same temperature of 800 °C and only different ambient deposition pressure (0.2, 0.002 mbar O_2, Table 2), the two layers sintered into one densified single layer (Figure 7 a). Cross-section micrograph of the sample with electrode deposited at 800 °C, 0.2 mbar O_2 and electrolyte at 600 °C, 0.002 mbar O_2 (Figure 7 b) illustrates the formation of porous, columnar electrode and dense electrolyte. However, the small thickness of the electrode may be the effect of a partial coalescence (intergrowth), with densification of the two layers at the interface. The microstructure of the two deposited layers resulted as intended, but the large difference in the deposition pressures (0.2 and 0.002 mbar O_2) leads to significant strain, with the partial delamination of the deposited layers from the substrate. A smaller difference in the deposition pressures (0.15 mbar at 800 °C and 0.007 mbar at 600 °C) resulted in a continuous, crack-free layer, but less porous microstructure of the cathode and a better densification of the cathode and electrolyte (Figure 7 c). Finally, a gradual decrease of the ambient pressure during deposition and lower temperature during electrolyte deposition (Table 2) generated porous cathode and dense electrolyte, without breaking and delamination of the deposited films from the substrate (Figure 7 d).

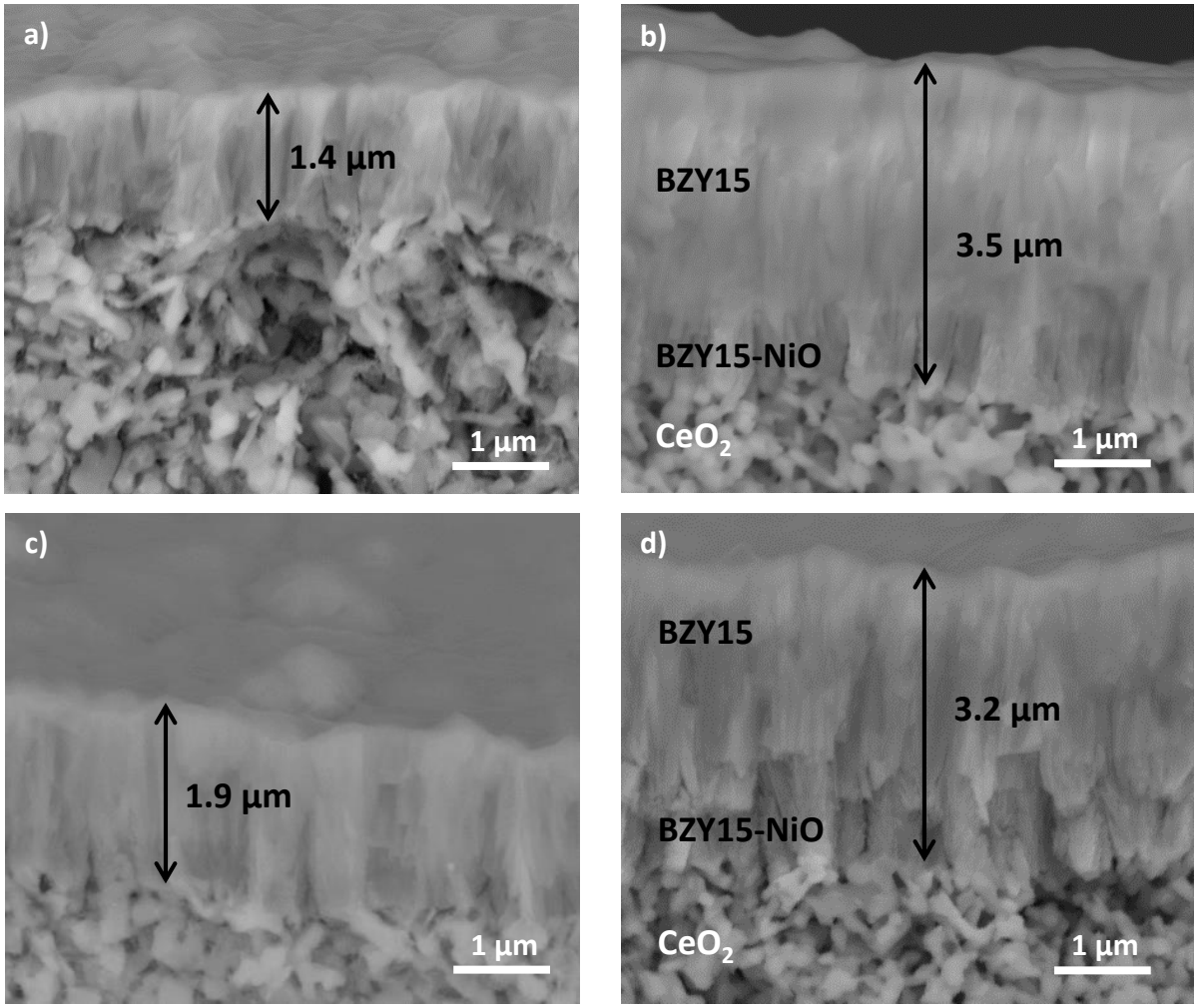

Figure 7 Cathode and electrolyte deposited on MS/CeO_2 substrate: a) – at the same temperature (800 °C) and different ambient pressures 0.2 and 0.002 mbar O_2; b) – at different temperatures (800, 600 °C) and at different pressure 0.2 and 0.002 mbar O_2; c) – at different temperatures (800, 600 °C) and different pressure 0.15 and 0.007 mbar O_2; d) – at different temperatures (800, 600 °C) and gradual decrease of the ambient pressures from 0.25, 0.15, 0.1, 0.02 and 0.002 mbar O_2.

MS/LSTN substrates were used for the deposition of BZY15 electrolyte alone or both, BZY-NiO cathode and electrolyte. Deposition parameters are listed in Table 2. A decrease in the substrate temperature from 800 to 600 °C would be beneficial for the metal support, thus a MS/LSTN – BZY15 sample was prepared at 600 °C. The deposition was carried out in two steps of O_2 pressure (0.1 and 0.02 mbar). The resulting film of BZY15 was not dense and showed columnar growth, with columns of ~4.7 µm, at 600 °C (Figure 8 a, b). The lower temperature and slightly higher roughness of the

substrate favoured growth of columns and only partial densification of BZY15. A second sample was prepared at 800 °C and 0.002 mbar O_2, and even though the MS/LSTN had surface roughness of ~1-3 µm, a much better densified BZY15 electrolyte film was obtained. Both surface and cross-section micrographs show good densification (Figure 8 c, d), without stress induced fissures. The sample confirmed that for a relatively rough initial surface and a porous substrate, higher substrate temperature and low ambient pressure improves the densification of BZY15. Cathode BZY-NiO and electrolyte were deposited on MS/LSTN substrate in a similar process as described for MS/CeO_2, with gradual decrease of the ambient pressure and different substrate temperatures (800, 600 °C) for cathode and electrolyte deposition, respectively. The cathode film was more porous than previously observed for MS/CeO_2/(BZY15-NiO)/BZY15 samples, with increased wide-to-length columns, as a consequence of applying only one pressure step (0.25 mbar O_2). A gradual densification of the columns to form the electrolyte (Figure 8 e) was achieved in three pressure steps (0.1, 0.02 and 0.002 mbar O_2) The surface micrograph depicts a relatively dense oxide layer, while grain boundaries delimitation is still visible, as an effect of the increased roughness of the MS/LSTN substrate (Figure 8 f).

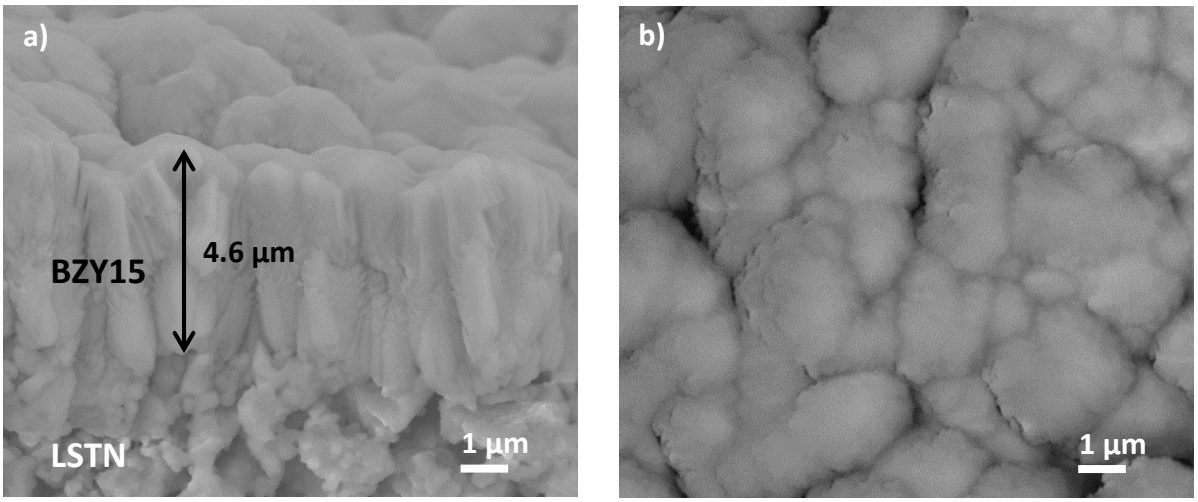

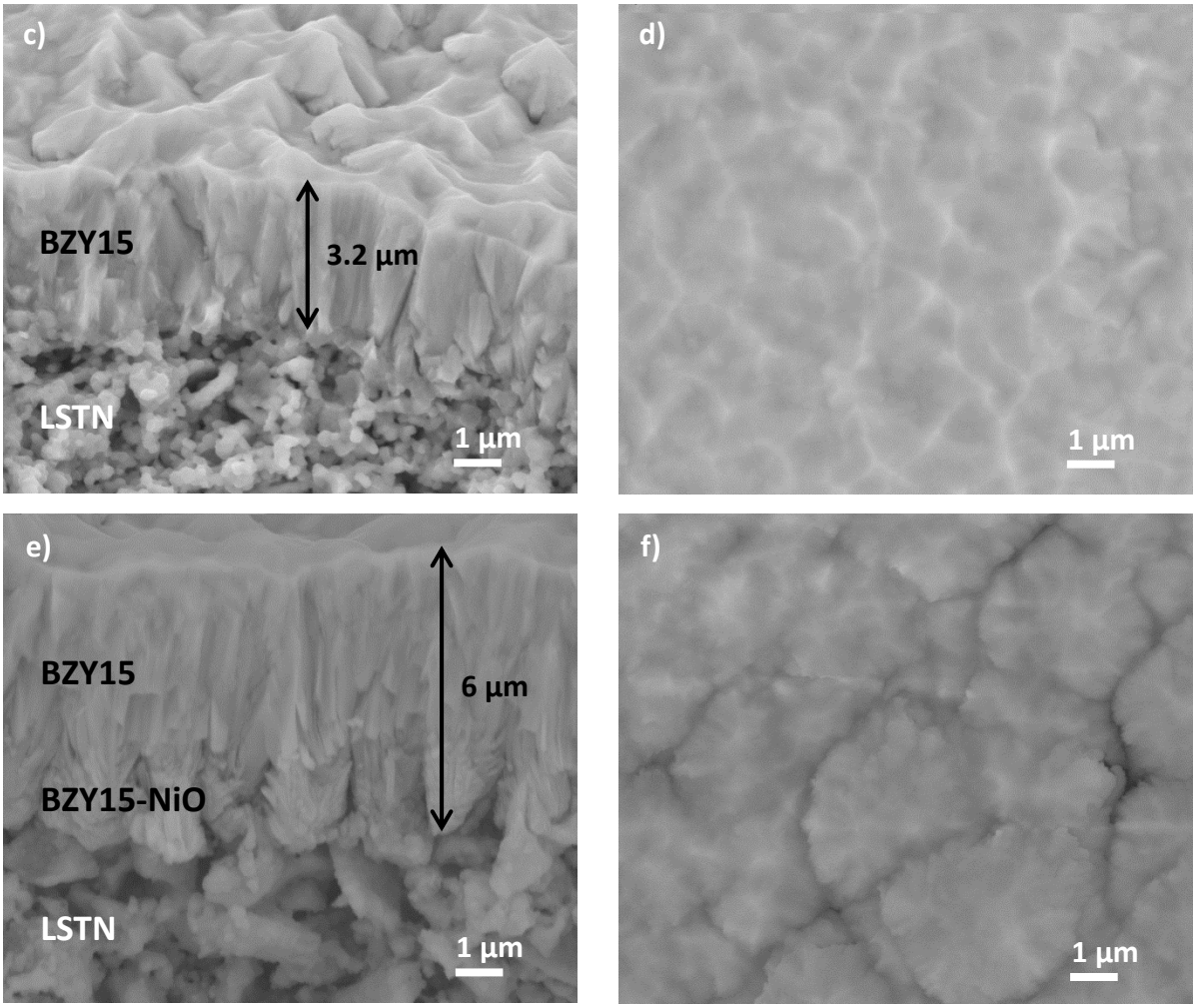

Figure 8 Cross-section and surface micrographs of BZY15 films deposited on MS/LSTN substrates at: a, b – 600 °C and two pressure steps (0.1 and 0.02 mbar O_2); c, d – 800 °C and 0.002 mbar O_2; e, f – cathode and electrolyte films deposited at different temperatures (800, 600 °C) and gradual decrease of the ambient pressures from 0.25 to 0.002 mbar O_2.

Films deposited on porous MS/ceramic substrates were dependent on surface roughness and the sintering ability of the ceramic layer under reducing conditions at temperatures < 1300 °C. The increased roughness and porosity of the MS/(BZY15-Ni) substrate caused an insufficient densification of the electrolyte layer. Films deposited on MS/CeO_2 and MS/LSTN developed appropriate microstructure, with porous BZY15-NiO and dense BZY15 layers.

Table 2 Deposition conditions for BZY15 and BZY-NiO films on porous MS/ceramic assemblies:

E (J/cm^2)	F (Hz)	P (mbar)	T (°C)	TSD (cm)	Substrate
1.6	7	0.25, 0.15	800	6	MS/(BZY-Ni)
	5	0.10, 0.02, 0.002	600	6	
1.4	5	0.20, 0.002	800	6	MS/CeO_2
1.4	5	0.20, 0.002	800, 600	6	MS/CeO_2
1.4	5	0.15, 0.007	800, 600	6	MS/CeO_2
1.6	7	0.25, 0.15	800	6	MS/CeO_2
	5	0.10, 0.02, 0.002	600	6	
1.4	5	0.002	800	6	MS/LSTN
1.6	5	0.007	800	6	MS/LSTN
1.6	5	0.10, 0.02	600	6	MS/LSTN
1.6	7	0.25	800	6	MS/LSTN
	5	0.10, 0.02, 0.002	600	6	

4 Conclusions

The microstructure of BZY15–NiO electrode and BZY15 electrolyte films made by PLD was studied as a function of deposition conditions, such as substrate temperature, ambient O_2 pressure and laser energy. The results showed that the deposition parameters play a major role in determining the porous or dense microstructure of the deposited films and were in a good agreement with models previously reported for films obtained by physical vapour deposition methods.

Deposition of BZY15–NiO electrode and BZY15 electrolyte films by PLD on metal supports has been implemented by employing an intermediary oxide layer to decrease roughness of the metal substrate.

The poor sintering of BZY15-Ni on the metal support in reducing atmosphere and temperature <1300 °C hindered the successful deposition of a dense electrolyte film. Thus, the MS/(BZY15-Ni)/(BZY15-NiO)/BZY15 cell was not further pursued for electrochemical tests.

Porous BZY15-NiO and dense BZY15 films were successfully deposited on metal supports with layered architectures e.g., MS/CeO_2/(BZY15-NiO)/BZY15 and MS/LSTN/(BZY15-NiO)/BZY15, thus avoiding the high temperature required for BZY15 sintering and exposure to air of the metal support. The sequence of porous film followed by a dense film was obtained by deposition at different temperatures to avoid the densification of the porous electrode and by applying a gradual decrease of the ambient pressure during deposition.

Some of the produced complete layered support-electrode-electrolyte structures were equipped with a top electrode and tested electrochemically. MS/CeO_2/(BZY15-NiO)/BZY15 cells showed a tendency to short-circuit during test while MS/LSTN/(BZY15-NiO)/BZY15 cells proved to be more robust; electrochemical tests will be described in more details elsewhere.

Acknowledgements

Financial support from the Research Council of Norway (RCN) through the ENERGIX program (Project No: 228819/E20) is gratefully acknowledged.

References

1. Ebbesen SD, Jensen SH, Hauch A, Mogensen MB (2014) High Temperature Electrolysis in Alkaline Cells, Solid Proton Conducting Cells, and Solid Oxide Cells. Chem Rev 114:10697–10734. doi: 10.1021/cr5000865

2. Laguna-Bercero MA (2012) Recent advances in high temperature electrolysis using solid oxide fuel cells: A review. J Power Sources 203:4–16. doi: 10.1016/j.jpowsour.2011.12.019

3. Steele BCH, Heinzel A (2001) Materials for fuel-cell technologies. Nature 414:345–352. doi: 10.1038/35104620

4. Fabbri E, Pergolesi D, Traversa E (2010) Materials challenges toward proton-conducting oxide fuel cells: a critical review. Chem Soc Rev 39:4355–4369. doi: 10.1039/B902343G

5. Shafi SP, Bi L, Boulfrad S, Traversa E (2015) Yttrium and Nickel Co-Doped BaZrO3 as a Proton-Conducting Electrolyte for Intermediate Temperature Solid Oxide Fuel Cells. ECS Trans 68:503–508. doi: 10.1149/06801.0503ecst

6. Kreuer KD (1997) On the development of proton conducting materials for technological applications. Solid State Ion 97:1–15. doi: 10.1016/S0167-2738(97)00082-9

7. Iwahara H, Yajima T, Hibino T, et al (1993) Protonic conduction in calcium, strontium and barium zirconates. Solid State Ion 61:65–69. doi: 10.1016/0167-2738(93)90335-Z

8. Babilo P, Haile SM (2005) Enhanced Sintering of Yttrium-Doped Barium Zirconate by Addition of ZnO. J Am Ceram Soc 88:2362–2368. doi: 10.1111/j.1551-2916.2005.00449.x

9. Nikodemski S, Tong J, O'Hayre R (2013) Solid-state reactive sintering mechanism for proton conducting ceramics. Solid State Ion 253:201–210. doi: 10.1016/j.ssi.2013.09.025

10. Tong J, Clark D, Hoban M, O'Hayre R (2010) Cost-effective solid-state reactive sintering method for high conductivity proton conducting yttrium-doped barium zirconium ceramics. Solid State Ion 181:496–503. doi: 10.1016/j.ssi.2010.02.008

11. Tong J, Clark D, Bernau L, et al (2010) Solid-state reactive sintering mechanism for large-grained yttrium-doped barium zirconate proton conducting ceramics. J Mater Chem 20:6333–6341. doi: 10.1039/C0JM00381F

12. Pergolesi D, Fabbri E, D'Epifanio A, et al (2010) High proton conduction in grain-boundary-free yttrium-doped barium zirconate films grown by pulsed laser deposition. Nat Mater 9:846–852. doi: 10.1038/nmat2837

13. Bi L, Boulfrad S, Traversa E (2015) Reversible solid oxide fuel cells (R-SOFCs) with chemically stable proton-conducting oxides. Solid State Ion 275:101–105. doi: 10.1016/j.ssi.2015.03.006

14. Bi L, Boulfrad S, Traversa E (2014) Steam electrolysis by solid oxide electrolysis cells (SOECs) with proton-conducting oxides. Chem Soc Rev 43:8255–8270. doi: 10.1039/C4CS00194J

15. Azad AK, Savaniu C, Tao S, et al (2008) Structural origins of the differing grain conductivity values in BaZr0.9Y0.1O2.95 and indication of novel approach to counter defect association. J Mater Chem 18:3414–3418. doi: 10.1039/B806190D

16. Evans A, Bieberle-Hütter A, Rupp JLM, Gauckler LJ (2009) Review on microfabricated micro-solid oxide fuel cell membranes. J Power Sources 194:119–129. doi: 10.1016/j.jpowsour.2009.03.048

17. Pergolesi D, Fabbri E, Traversa E (2010) Chemically stable anode-supported solid oxide fuel cells based on Y-doped barium zirconate thin films having improved performance. Electrochem Commun 12:977–980. doi: 10.1016/j.elecom.2010.05.005

18. Evans A, Martynczuk J, Stender D, et al (2015) Low-Temperature Micro-Solid Oxide Fuel Cells with Partially Amorphous La0.6Sr0.4CoO3-δ Cathodes. Adv Energy Mater 5:n/a-n/a. doi: 10.1002/aenm.201400747

19. Heiroth S, Frison R, Rupp JLM, et al (2011) Crystallization and grain growth characteristics of yttria-stabilized zirconia thin films grown by pulsed laser deposition. Solid State Ion 191:12–23. doi: 10.1016/j.ssi.2011.04.002

20. Chang I, Paek JY, Cha SW (2015) Parametric study of Y-doped BaZrO3 thin film deposited via pulsed laser deposition. J Vac Sci Technol A 33:021515. doi: 10.1116/1.4905775

21. Infortuna A, Harvey AS, Gauckler LJ (2008) Microstructures of CGO and YSZ Thin Films by Pulsed Laser Deposition. Adv Funct Mater 18:127–135. doi: 10.1002/adfm.200700136

22. Chao C-C, Hsu C-M, Cui Y, Prinz FB (2011) Improved Solid Oxide Fuel Cell Performance with Nanostructured Electrolytes. ACS Nano 5:5692–5696. doi: 10.1021/nn201354p

23. Kerman K, Lai B-K, Ramanathan S (2011) Pt/Y0.16Zr0.84O1.92/Pt thin film solid oxide fuel cells: Electrode microstructure and stability considerations. J Power Sources 196:2608–2614. doi: 10.1016/j.jpowsour.2010.10.068

24. Noh H-S, Park J-S, Son J-W, et al (2009) Physical and Microstructural Properties of NiO- and Ni-YSZ Composite Thin Films Fabricated by Pulsed-Laser Deposition at T≤700°C. J Am Ceram Soc 92:3059–3064. doi: 10.1111/j.1551-2916.2009.03362.x

25. Noh H-S, Son J-W, Lee H, et al (2010) Suppression of Ni agglomeration in PLD fabricated Ni-YSZ composite for surface modification of SOFC anode. J Eur Ceram Soc 30:3415–3423. doi: 10.1016/j.jeurceramsoc.2010.07.035

26. Noh H-S, Yoon KJ, Kim B-K, et al (2014) The potential and challenges of thin-film electrolyte and nanostructured electrode for yttria-stabilized zirconia-base anode-supported solid oxide fuel cells. J Power Sources 247:105–111. doi: 10.1016/j.jpowsour.2013.08.072

27. Arrivé C, Delahaye T, Joubert O, Gauthier G (2013) Exsolution of nickel nanoparticles at the surface of a conducting titanate as potential hydrogen electrode material for solid oxide electrochemical cells. J Power Sources 223:341–348. doi: 10.1016/j.jpowsour.2012.09.062

28. Stange M, Denonville C, Larring Y, et al (2013) Coating Developments for Metal-Supported Solid Oxide Fuel Cells. ECS Trans 57:511–520. doi: 10.1149/05701.0511ecst

29. Abràmoff MD, Magalhães PJ, Ram SJ (2004) Image processing with ImageJ. Biophotonics Int 11:36–42.

30. Schneider CA, Rasband WS, Eliceiri KW (2012) NIH Image to ImageJ: 25 years of image analysis. Nat Methods 9:671–675.

31. Iguchi F, Sata N, Yugami H (2010) Proton transport properties at the grain boundary of barium zirconate based proton conductors for intermediate temperature operating SOFC. J Mater Chem 20:6265–6270. doi: 10.1039/C0JM00443J

32. Serra JM, Meulenberg WA (2007) Thin-Film Proton BaZr0.85Y0.15O3 Conducting Electrolytes: Toward an Intermediate-Temperature Solid Oxide Fuel Cell Alternative. J Am Ceram Soc 90:2082–2089. doi: 10.1111/j.1551-2916.2007.01677.x

33. Ricote S, Bonanos N, Manerbino A, et al (2014) Effects of the fabrication process on the grain-boundary resistance in BaZr0.9Y0.1O3−δ. J Mater Chem A 2:16107–16115. doi: 10.1039/C4TA02848A

34. Muecke UP, Akiba K, Infortuna A, et al (2008) Electrochemical performance of nanocrystalline nickel/gadolinia-doped ceria thin film anodes for solid oxide fuel cells. Solid State Ion 178:1762–1768. doi: 10.1016/j.ssi.2007.10.002

35. Muecke UP, Graf S, Rhyner U, Gauckler LJ (2008) Microstructure and electrical conductivity of nanocrystalline nickel- and nickel oxide/gadolinia-doped ceria thin films. Acta Mater 56:677–687. doi: 10.1016/j.actamat.2007.09.023

36. Podpirka A, Balakrishnan V, Ramanathan S (2013) Heteroepitaxy and crystallographic orientation transition in La1.875Sr<span

class=“sub”>0.125NiO4 thin films on single crystal SrTiO3. J Mater Res 28:1420–1431. doi: 10.1557/jmr.2013.121

37. Viswanath B, Ko C, Ramanathan S (2011) Thickness-dependent orientation evolution in nickel thin films grown on yttria-stabilized zirconia single crystals. Philos Mag 91:4311–4323. doi: 10.1080/14786435.2011.608086

38. Thornton JA (1974) Influence of apparatus geometry and deposition conditions on the structure and topography of thick sputtered coatings. J Vac Sci Technol 11:666–670. doi: 10.1116/1.1312732

39. Plonczak P, Bieberle-Hütter A, Søgaard M, et al (2011) Tailoring of LaxSr1-xCoyFe1-yO3-δ Nanostructure by Pulsed Laser Deposition. Adv Funct Mater 21:2764–2775. doi: 10.1002/adfm.201100251

40. Tsekouras G, Neagu D, Irvine JTS (2012) Step-change in high temperature steam electrolysis performance of perovskite oxide cathodes with exsolution of B-site dopants. Energy Environ Sci 6:256–266. doi: 10.1039/C2EE22547F

41. Irvine JTS, Neagu D, Verbraeken MC, et al (2016) Evolution of the electrochemical interface in high-temperature fuel cells and electrolysers. Nat Energy 1:15014. doi: 10.1038/nenergy.2015.14